

Magnetization profile across Au-covered bcc Fe films grown on a vicinal surface of Ag(001) as seen by x-ray resonant magnetic reflectivity

Emmanuelle Jal,¹ Maciej Dąbrowski,² Jean-Marc Tonnerre,^{1,*} Marek Przybylski,^{2,3,†} Stéphane Grenier,¹ Nicolas Jaouen,⁴ and Jürgen Kirschner^{2,5}

¹*Institut Néel, CNRS and Université Joseph Fourier, 25 rue des Martyrs, BP166, 38042 Grenoble Cedex 9, France*

²*Max-Planck-Institut für Mikrostrukturphysik, Weinberg 2, 06120 Halle, Germany*

³*Academic Centre of Materials and Nanotechnology, and Faculty of Physics and Applied Computer Science, AGH University of Science and Technology, al. Mickiewicza 30, 30-059 Kraków, Poland*

⁴*Synchrotron SOLEIL, Saint-Aubin, BP 48, 91192 Gif-sur-Yvette Cedex, France*

⁵*Institut für Physik, Martin-Luther-Universität Halle-Wittenberg, 06099 Halle, Germany*

(Received 15 January 2013; published 21 June 2013)

We report on the local magnetic properties of ultrathin bcc Fe films grown on a Ag(1,1,6) stepped surface and covered by a Au layer. We determined the structure of the multilayer stack and the depth-resolved magnetic profile for 5.9 and 13.5 monolayer (ML) thick films. The experiments were carried out on magnetically saturated samples by soft x-ray resonant magnetic reflectivity using both circularly and linearly polarized x rays and two different acquisition configurations. Our results indicate a 20% enhancement of the magnetic moment in the first 2–3 ML of Fe at both interfaces. A comparison of the magnetization profile for Fe films grown on a flat Ag(001) surface indicates a very similar effect and does not reveal any difference regarding the method's accuracy.

DOI: 10.1103/PhysRevB.87.224418

PACS number(s): 75.70.-i

I. INTRODUCTION

Any change in the electronic states' occupation and lower atomic coordination at the surface/interface—resulting in band narrowing—changes the surface magnetic moment.¹ From an atomic perspective, these moments should increase at the surface/interface, which has a dimensionality somewhere between bulk and monolayer. However, from a statistical mechanics perspective, the average moment at a nonzero temperature should decrease. For surfaces, the loss of magnetic neighbors in a magnetic surface indicates a weakening of the exchange interaction resulting in a stronger decrease of the magnetic order with temperature.

Changes of the magnetic moment at ferromagnetic layer interfaces have been predicted for Fe layers in contact with Ag and Au layers. However, they were only indirectly observed. Theoretically, the magnetic moment was predicted to increase at the Fe/Ag(001) and Fe/Au(001) interfaces up to 2.98–3.01 and 2.97 μ_B , respectively (i.e., no significant difference was found between the degree of enhancement for Fe/Ag and Fe/Au interfaces).^{2–4} The depth profile of magnetic hyperfine field B_{hf} near the Fe/Ag interface was reported by Tyson *et al.*⁵ for epitaxial Fe(110) films on Ag(111). An increase of the ground-state B_{hf} , i.e., $B_{\text{hf}}(0)$, at the interface was found and interpreted in terms of magnetic moment enhancement. A more detailed, monolayer-resolution conversion electron Mössbauer experiment (CEMS) analysis of the Ag/Fe interface in films of well-defined structures was undertaken by Korecki *et al.*⁶ Here a slightly increased value of $B_{\text{hf}}(0)$ in comparison to the film center was observed for the Fe interfacing layer decreasing monotonically to the bulk value over a few atomic layers. At room temperature (RT) the $B_{\text{hf}}(\text{RT})$ at the Fe/Ag interface is smaller than the bulk $B_{\text{hf}}(\text{RT})$ due to the magnetization's temperature dependence. This dependence is at least two times stronger at the interface if compared to the film center. Note that this temperature effect could be weaker the thinner the layers become. In contrast, a monotonic increase of B_{hf}

towards the Au/Fe interface was observed at RT. A ground-state value of $B_{\text{hf}}(0) = 36.6$ T at the Au/Fe interface was reported.⁷ It is assumed that a modification of the valence electron contribution is responsible for the minor changes of B_{hf} between Fe layers facing Ag and Au coatings. Otherwise, the increased value of the magnetic moment in both cases is expected to be approximately the same.⁴ There are also some experimental evidences on the increased magnetic moment in ultrathin Fe films deposited on Ag(001) and covered by Au.^{8–10}

There are several magnetometric methods available, which are applicable *in situ* under ultrahigh vacuum (UHV) conditions, like the torsion oscillatory magnetometer (TOM) or the superconducting quantum interference device (SQUID), which are sensitive enough to detect monolayer (ML) signals. However, since these are integral methods and feature no spatial resolution, they cannot be used for local investigations (e.g., sensitive to surface magnetization). Thus, our knowledge about surface magnetism stems from surface sensitive techniques, measuring quantities not directly related to the magnetic moment. Complications arise if a spatial resolution (on a subnanometer level) is required or a buried interface needs to be probed. In the last two decades progress has been made with the advent of the x-ray magnetic circular dichroism (XMCD) technique using synchrotron radiation and applied under different conditions (absorption, photoemission) to create high magnetic sensitivity with element and orbital selectivity. Despite being also an integrating technique, attempts have been made to obtain a spatial resolution with XMCD—either by using samples of different thicknesses (cf. e.g., Ref. 11)—or by detecting electrons for various emergent angles (i.e., emerging from various depths¹²). However, these two methods are indirect. Both assume the same magnetic distribution, regardless of the layer thickness. They also extrapolate values to interfaces with the thickness dependence of the average signal's variation. Moreover, the number of detected electrons emerging from the sample must be corrected depending on the depth from which they originate.

Then, only two quantities can be measured: (1) a magnetic hyperfine field (B_{hf}) that can be probed layer-by-layer, due to the isotope specificity of the Mössbauer spectroscopy,¹³ or (2) a magnetic moment as a parameter, influencing diffraction or reflectivity, that can be either probed with neutrons (e.g., Ref. 14) or synchrotron radiation at the absorption edge of the magnetic element using polarized x-rays.^{15,16} X-ray resonant magnetic reflectivity (XRMR), a reciprocal space technique intrinsically providing a subnanometer spatial resolution, has proven to be a powerful tool for probing the magnetic properties of ultrathin films. Initially the investigation of magnetic profiles by XRMR mainly focused either on layers sandwiched between two ferromagnetic layers,^{17–21} or antiferromagnetic layers exhibiting a net magnetization related to some ferromagnetic ordering or canting. In the latter case two different magnetization sources were identified: exchange coupling with a ferromagnetic layer,^{22–24} or a charge transfer across the interface from a nonmagnetic layer.²⁵ Recently two studies were focused on the magnetic structure and on the layer-resolved temperature dependence of the magnetization inside the complex antiferromagnetic Fe/Cu(001) structure.^{26,27} Among the studies on magnetic profiles within a ferromagnetic layer^{15,28} only a few report on the magnetic moment enhancement near the interface.^{29,30}

In this work we report on the investigation of a Au/Fe/Ag(1,1,6) system by XRMR. The most important property of the Fe layer on the Ag vicinal surface and covered by Au is the thickness dependence of the in-plane easy magnetization axis, which oscillates at low temperature from along the steps to perpendicular to the steps.^{31,32} The oscillatory magnetic anisotropy originates from quantum well states (QWS) formed in Fe ultrathin films due to the d -electron confinement along the growth direction. The formation of QWS indicates a high structural quality of the films as well as chemical sharpness of the interfaces.³³ The aim of our investigations is to better understand the origin of this oscillation. As part of this study we investigated the Fe depth-resolved profile of saturated magnetization at the Fe L edge using soft x rays. Here we provide direct evidence for an interfacial enhancement up to 20% with respect to the bulk value of a bcc Fe thin film's magnetization. We determined the depth-resolved magnetic profile with a subnanometer spatial resolution for 5.9 and 13.5 ML Fe films.

II. EXPERIMENTAL DETAILS

The Au/Fe/Ag(1,1,6) sample was prepared in a multichamber ultrahigh vacuum (UHV) system with a pressure below 2×10^{-10} mbar during Fe deposition. The Ag(1,1,6) substrate was prepared in cycles of 1 keV Ar ion sputtering and subsequent annealing at 500 °C. This surface preparation procedure yields vicinal surfaces, characterized by regular monoatomic steps, with the step edges oriented along the Ag[110] crystalline direction.³² Low-energy electron diffraction imaging reveals sharp double-split diffraction spots, which are characteristic for a vicinal surface and thus confirms the expected terrace width of 0.86 nm for Ag(1,1,6). The Fe film was grown at RT, by molecular beam epitaxy, as a wedge sample with a slope of 1 ML/mm, and with a thick shoulder for determining the wedge position. The Fe grew in a 45° rotated bcc phase on the Ag(1,1,6) surface, with the in-plane lattice parameter

expanded by 0.8% to match the Ag lattice parameter. After the growth process, the film was annealed at 150 °C for 30 min to improve the surface morphology. To avoid contamination during the soft-XRMR measurements, the Fe wedge was capped with a 15 ML thick Au layer. The system was fully characterized by *in situ* longitudinal magneto-optical Kerr effect (MOKE) measurements.^{31,34} In our study we measured two different areas (latter on called samples), with nominal Fe thicknesses 5.7 and 13.75 ML, to compare the magnetic profile. The MOKE measurements have shown that the easy magnetization axis is perpendicular to the steps for the 5.7 ML of Fe and parallel to the steps for the 13.75 ML Fe at $T = 20$ K.

The soft-XRMR measurements were carried out at the RESOXS end station³⁵ on the SEXTANTS beamline³⁶ at SOLEIL in Saclay, France. The experiments were performed under UHV condition in order to avoid absorption of the soft x-rays by air and high contamination of the surface at low temperatures. The beam size is around 200 μm^2 which allows a thickness resolution of 0.2 ML on our wedge sample. The method combines the spatial resolution of x-ray reflectivity and the chemical selectivity of x-ray circular magnetic dichroism. The magnetic contrast in the reflectivity measurements occurs at an absorption edge. The data have been collected with incident photon energy in the vicinity of the Fe L_3 edge. This edge lies at 706.8 eV in the soft x-ray range (e.g., 200–2000 eV) and corresponds to a transition from the $2p_{3/2}$ level to the $3d$ states. The measurements are therefore sensitive to the Fe $3d$ magnetic moment. It is a photon-in photon-out process leading to a change of the reflected photons' polarization state, with respect to the incoming photons after interacting with the Fe magnetic layer. In the XRMR experiments the angular dependence of the specular reflectivity is collected either for two opposite orientations of an applied magnetic field, or for two opposite helicities of the incoming beam. Just as the regular specular x-ray reflectivity is sensitive to the electronic density distribution along the growth axis, the angle dependent changes, occurring in the two intensities I^+ and I^- , are linked to the distribution of the Fe magnetization across the layer. The reflectivity curves were recorded in the $\theta/2\theta$ scan mode (Fig. 1) at $T = 20$ K. The sample is mounted with the steps perpendicular to the diffraction plane (Fig. 1). There are several experimental approaches available to obtain the reflected intensities I^+ and I^- . In this work we used two different

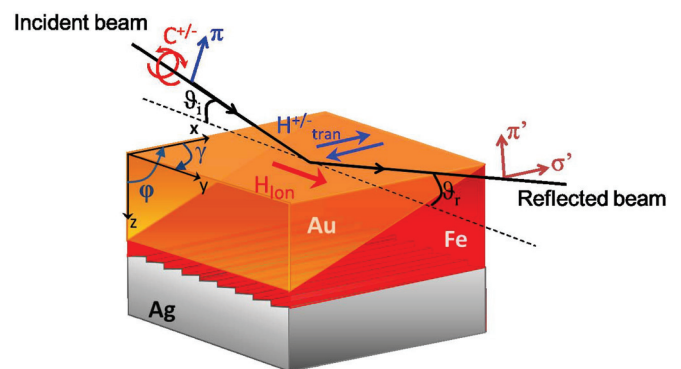


FIG. 1. (Color online) Sketch of the sample showing the orientation of the Fe wedge with respect to the Ag step edges, and experimental configurations.

experimental configurations. In the first, Cpm, an external magnetic field is applied parallel to the scattering plane along the sample's surface (longitudinal direction). In the second one, called Pi, a π linear polarization (i.e., within the scattering plane) of the incoming beam is used for two different orientations of the magnetic field applied along the steps (transverse direction). These configurations are depicted in Fig. 1. All experiments discussed below are performed at saturation by applying a field of $\mu_0 H = 0.05$ T determined from MOKE measurements.

III. RESULTS

In order to probe the sample's net magnetization, the magnetic asymmetry $A = (I^+ - I^-)/(I^+ + I^-)$ is analyzed using a code developed by the Institut Néel.³⁷ First, the structural parameters, layer thickness, and roughness are determined by refining the reflectivity curves obtained with incident photon energy away from the edge (at 680 eV) to strongly reduce the effects of the energy dependent resonant terms in the scattering factor. The energy dependent imaginary correction to the charge scattering factor was determined from x-ray absorption data obtained from thick Fe films and scaled in electron units using the Chantler's tables away from the edge.¹⁵ The energy dependence of the real part was derived by using the Kramers-Kronig relationship applied to the scaled experimental absorption data extended far below and above the edge as suggested in Ref. 38. At -26.8 eV below the edge, while the resonant contribution of f'' is negligible, it is however necessary to take into account a small f' contribution. Second, while keeping the structural parameters fixed, the magnetic asymmetry is refined by adjusting a quantity proportional to the magnetic moment. Its amplitude and orientation are defined by the magnetic scaling factor msf and the two angles φ and γ (Fig. 1). To meet the experimental asymmetry, the magnetic layer can be divided into several magnetic slices allowing the derivation of a depth-resolved magnetic profile. Although XRMR does not measure magnetization directly, the method probes changes in the complex atomic scattering factor or refractive index, which are sensitive to the magnetic moment in each slice.¹⁵ The imaginary part of this energy dependent term of the scattering factor is related to the amplitude of the XMCD signal and the real part to its Kramers-Kronig transform.³⁹ Sum rules applied to the XMCD signal allow the link to the magnetic moment amplitude.⁴⁰ In the quantitative analysis, the amplitude of the magnetization dependent terms in the scattering atomic factor is modified by adjusting the msf , which is expressed in a referent Fe magnetic moment amplitude mm_0 . The XMCD data used in this analysis come from thick Fe films and the application of sum rules yields $mm_0 = 2.1 \mu_B$.⁴⁰ Subsequently, the relevance of the XMCD reference was confirmed by XMCD data measured on the Au/Fe(8 ML)/Ag(1,1,6) at the DEIMOS beamline of SOLEIL.⁴¹ Although those data led to a very good superimposition of the XMCD signals, they were not used to determine the charge and magnetic resonant parameters because of the presence of an additional contribution, namely the Ag M_1 absorption edge that precludes a good scaling to be done. At the end, a refined msf value equal to one at a certain depth corresponds to a magnetic moment of $2.1 \mu_B$ per Fe atom. This parameter is allowed to vary from 0 to 1.5 (i.e., from 0 to $3.15 \mu_B$) in the procedure.

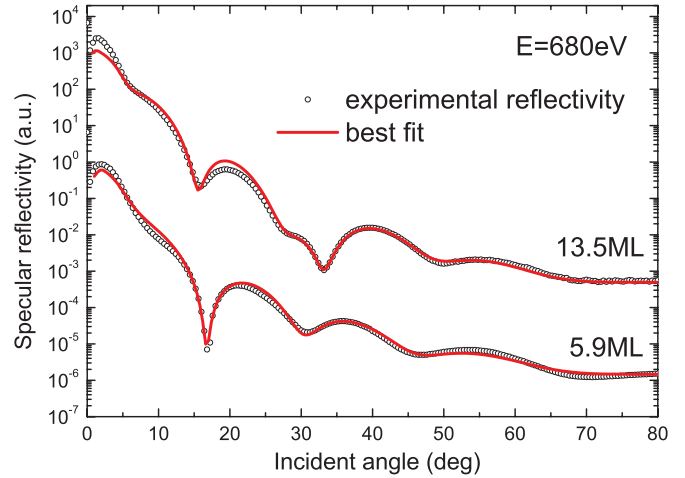


FIG. 2. (Color online) X-ray specular reflectivity for Fe films 5.9 and 13.5 ML thick measured at RT at 680 eV using circularly polarized incident photons (dots), and best fit (line).

Figure 2 shows reflectivity curves for both samples obtained with circularly polarized photons at 680 eV. A very good agreement between the experiment and the best fit is observed for both Fe thicknesses. The structural parameters are summarized in Table I. The density was kept equal to the bulk value since attempts to refine these values did not improve the result. The roughness parameters correspond to the width of a Gaussian broadening of the interface between two chemically different media, treated through an error function as described in Ref. 37. By considering the bcc Fe(001) d -spacing (1.4332 \AA) value for a Fe monolayer thickness, a good agreement is observed between the experimental (e.g., 13.5 and 5.9 ML) and the nominal values (13.75 and 5.7 ML, respectively) of the Fe films thickness (while the Au film corresponds to 17 ML rather than 15 ML nominally).

Figure 3 shows the experimental magnetic asymmetry (A) obtained at 705.5 eV for an Fe thickness of 13.5 ML in both Cpm and Pi configurations. The asymmetries exhibit very different shapes. The normalization of the intensity difference by the sum imposes the dependence on the shape of the reflectivity. Not only the charge reflectivity differs with π or circularly polarized incident beam due to the $\cos(2\theta)$ dependence of the reflected photons in the π - π channel. Also a change of the magnetization's orientation, from longitudinal in the Cpm configuration to transverse in the Pi configuration, modifies the asymmetry's angular dependence.⁴² The ability to refine such a large difference with the same model allows a reliable determination of the depth-resolved magnetic profile.

TABLE I. Structural parameters obtained from the fit of experimental reflectivity curves made at 680 eV for both 13.5 ML of Fe and 5.9 ML of Fe.

	Density (mol cm ⁻³)	Thickness (\AA)		Roughness (\AA)	
		13.5 ML	5.9 ML	13.5 ML	5.9 ML
Au	0.098	36.4 ± 0.4	37.0 ± 0.2	3.6 ± 0.5	3.4 ± 0.3
Fe	0.141	19.4 ± 0.3	8.4 ± 0.1	2.1 ± 0.6	2.0 ± 0.1
Ag	0.097	—	—	2.2 ± 0.7	0.8 ± 0.3

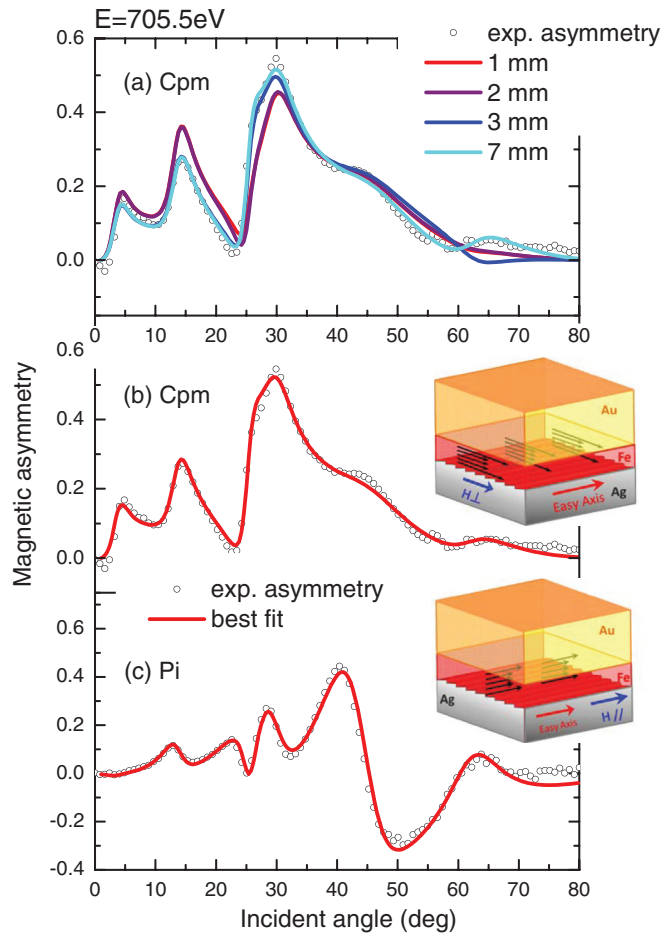


FIG. 3. (Color online) Magnetic asymmetry for 13.5 ML of Fe deposited on Ag(1,1,6) and covered by 17 ML of Au obtained by soft XRRM at 705.5 eV. (a) Evolution of the theoretical asymmetry as a function of the number of magnetic slices mm for an asymmetry ratio obtained in a Cpm configuration. (b) Experimental and theoretical asymmetry ratio obtained for $mm = 5$ in the Cpm configuration. (c) Experimental and theoretical asymmetry ratio obtained for $mm = 5$ in the Pi configuration. Insets of (b) and (c) show a sketch of the depth magnetization profile obtained for the Cpm and Pi configurations, respectively.

The structural parameters obtained at 680 eV are used to reproduce the reflectivity curves collected at 705.5 eV. It is sometimes necessary to make further slight adjustments to improve the agreement between experimental curves and the calculated ones. The agreement is achieved by restricting the parameter variation inside the error bars obtained at 680 eV. The magnetic asymmetry is then fitted by optimizing the magnetic parameters. All measurements are carried out under saturation condition with magnetic field applied in the sample plane, $\varphi = 90^\circ$ in both configurations, and $\gamma = 90^\circ$ or $\gamma = 0^\circ$ in the Cpm and Pi configuration, respectively. Therefore, only the msf is refined. This parameter is optimized within the constraint of a lower and upper limit, preventing the fit from giving unrealistic results. For the Cpm configuration, considering a homogeneous magnetization in the entire Fe layer, a single magnetic slice 19.4 Å thick gives the fit labeled $mm = 1$ (red line) in Fig. 3(a). The observed discrepancy between the experiment and the fit can be an indication of

magnetic inhomogeneity across the Fe layer.¹⁵ This hypothesis is reinforced by the fact that a further refinement of A , allowing the structural parameters to change, only slightly improves the asymmetry. This can result, however, in wrong structural parameters leading to very different reflectivity curves. This prompts us to successively divide the Fe layer into an increasing number of magnetic slices, $mm = 2, 3, 5, 7$. Here we point out that the possibility of magnetic roughness different from the structural one is not taken into account through a specific parameter (as in Ref. 43) but rather through the slicing procedure discussed afterwards that enables us to probe either a reduction or an enhancement of the magnetization. The Fe layer is first divided into $mm = 2$ slices of equal thicknesses. The two msf values are fitted independently from each other and the result is displayed in Fig. 3(a) (purple line). It shows almost no improvement in the agreement between theoretical and experimental asymmetry. When the Fe layer is divided into $mm = 3$ magnetic slices (blue line), the quality of the fit is further enhanced for reflected angles θ below 40° . But it is not satisfactory at larger angles. Increasing the number of magnetic Fe slices up to $mm = 7$ leads to a better agreement between theoretical and experimental asymmetry. However, the improvement is not so significant for six or seven magnetic slices {light blue line in Fig. 3(a)} when compared to the already very good agreement obtained with only $mm = 5$ magnetic slices [Fig. 3(b)]. Therefore, in order to minimize the number of free parameters, the magnetic analysis of asymmetries collected for two acquisition configurations is performed with an Fe layer divided into $mm = 5$ equally thick magnetic slices. The best fit, shown in Fig. 3(b), is obtained for the msf values of 1.16/1.03/1.05/0.98/1.16 from the Au layer to the Ag substrate. This magnetic profile indicates an enhancement of the magnetic moment at both interfaces.

In order to test the depth magnetic profile's robustness, derived from the Cpm configuration, the asymmetry recorded in the Pi configuration is analyzed. Here the magnetic moments are aligned along the steps, which is also along the easy magnetization axis. Figure 3(c) shows that a good agreement is obtained between experimental and theoretical curves with the following msf values: 1.20/1.09/1.05/1.03/1.16. This distribution of msf confirms the enhancement of the magnetic moment at the interfaces and gives approximate indications on the error bars. The measurements' analysis carried out at another energy close to the resonance (706.5 eV) for both configurations, leads to complementary magnetic profiles with slightly different msf values. All these results allow us to derive the following average profile: $1.22 \pm 0.07/1.03 \pm 0.06/1.05 \pm 0.06/1.04 \pm 0.06/1.18 \pm 0.04$. The same experiment was also carried out at RT resulting in the spectra almost identical to the spectra measured at $T = 20$ K and shown in Fig. 3.

Fig. 4 shows how the calculated magnetization profile evolves with different models: (i) starting from the decrease of the magnetization at the interfaces (i.e., $msf = 0.8/1/1/1/0.8$ and $msf = 0.9/1/1/1/0.9$), (ii) along with the homogeneous magnetization across the film (i.e., $msf = 1/1/1/1/1$ and $msf = 1.1/1.1/1.1/1.1/1.1$), and finally (iii) assuming the increased magnetization at the interfaces (i.e., $msf = 1.1/1/1/1/1.1$ or $1.2/1/1/1/1.2$ or

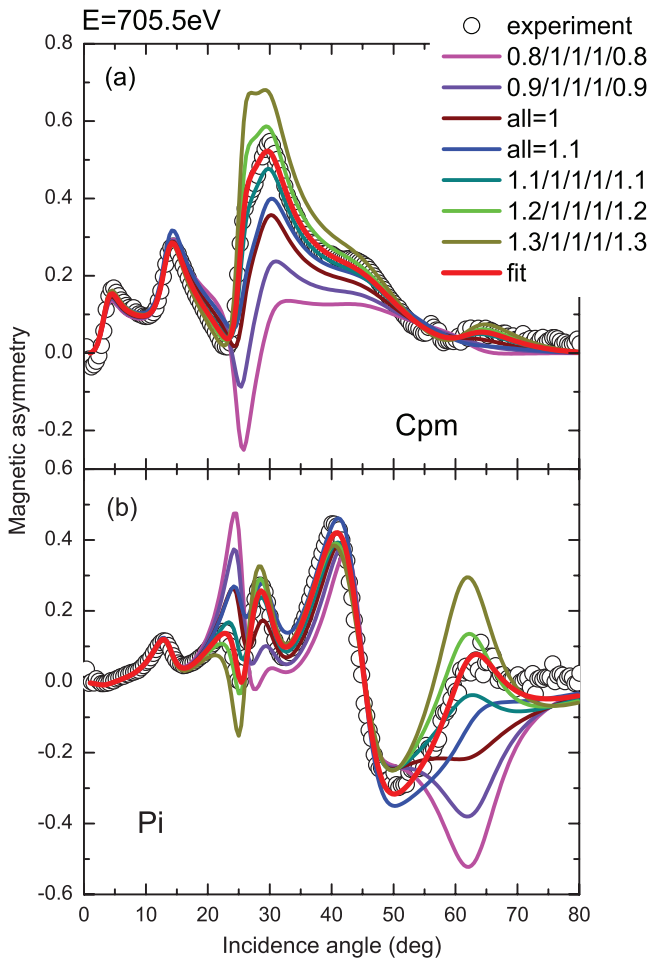


FIG. 4. (Color online) Magnetic asymmetry for 13.5 ML of Fe deposited on Ag(1,1,6) and covered by 17 ML of Au obtained by soft XRM R at 705.5 eV. Evolution of the theoretical asymmetry as a function of the msf profile for $mm = 5$ in the (a) Cpm and (b) Pi configurations, respectively.

1.3/1/1/1/1.3). The figure proves that even qualitatively the increased magnetization at the interfaces is the only way to properly describe the spectra measured experimentally. Additionally, Fig. 4 highlights the strong interest to use both Cpm and Pi configurations. Indeed, when the sensitivity to the different model assumptions is weak at large angle in the Cpm configuration, it is possible to observe a larger sensitivity in the Pi configuration due to the different angular dependence of the magnetic asymmetry.⁴²

The 20% enhancement of the magnetic moment at the interfaces is observed over a thickness of 3.88 Å (the size of the slices), which corresponds to 2 to 3 ML. This is the limit of the spatial resolution at the Fe L_3 edge with data ranging from 0° to 85° (corresponding to the scattering vectors ranging from 0 to 0.7 Å⁻¹) and for the layers about 20 Å thick as previously observed.¹⁵ For ferromagnetic arrangement, soft XRM R cannot resolve the Fe magnetic profile below this limit. Nevertheless, it confirms the interface character of the enhancement. Since our fitted value is averaged over the slice thickness, it cannot be excluded that the enhancement is even stronger at the interface atomic layer. In order to resolve the

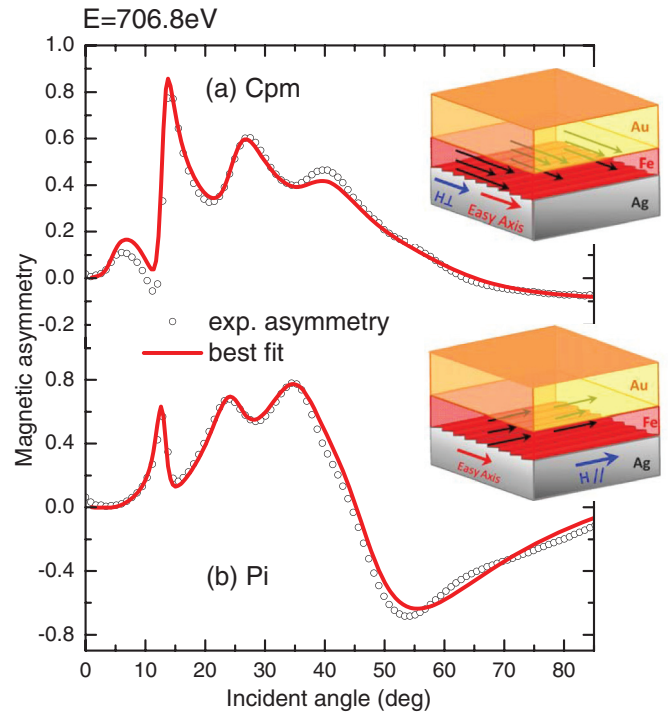


FIG. 5. (Color online) Magnetic asymmetry for 5.9 ML of Fe deposited on Ag(1,1,6) and covered by 17 ML of Au obtained by soft XRM R at 706.8 eV. (a) Experimental and theoretical asymmetry ratio obtained for $mm = 3$ in the Cpm configuration. (b) Experimental and theoretical asymmetry ratio obtained for $mm = 3$ in the Pi configuration.

issue of the enhanced magnetization extension, soft-XRM R measurements were performed on a thinner Fe layer (5.9 ML).

Figure 5 displays the experimental asymmetry curves obtained at 706.8 eV for an Fe thickness of 5.9 ML in both Cpm [Fig. 5(a)] and Pi [Fig. 5(b)] configurations. They show similar features as those obtained for the 13.5 ML sample: (i) positive asymmetry for the Cpm configuration and (ii) change of sign at approximately 45° for the Pi configuration. However, the shape differs because of dissimilar oscillations in the reflectivity curve. These dissimilarities are caused by the reduced thickness of the Fe layer. The analysis is performed by defining an optimized number of magnetic slices which is found to be $mm = 3$, with a thickness of 2.8 Å corresponding to 2 ML, i.e., the magnetic moment values are expected to be determined with an improved localization since they are integrated over the slices thinner than those in the 13.5 ML thick Fe film. For the Cpm and Pi configurations, Figs. 5(a) and 5(b), respectively, display a good agreement between the experimental curves and the best fit. The derived msf are $1.34 \pm 0.1/1.05 \pm 0.06/1.39 \pm 0.15$ from Au/Fe to Fe/Ag interfaces. This confirms the interfacial magnetic moments' enhancement and gives a better agreement (when the integration is limited to 2 ML) with several calculations predicting the largest enhancement in the first atomic layer.

The depth resolved interfacial enhancement derived from soft XRM R can be compared to theoretical and experimental results found in the literature. However, it is required to consider the fact that usually the magnetic moment enhancement

at Fe/Ag interfaces is either theoretically predicted or experimentally derived for Fe layers on a flat Ag(001) surface. As a high step density for Ag(1,1,6) surface leads to a lowering of the atomic coordination at the interfaces, we are prompted to evaluate the additional enhancement caused by the steps before making further comparisons between theoretical and experimental data. Therefore, the soft-XRMR approach was applied to an Fe layer deposited on a flat Ag(001) surface. The experiments were performed on an Au/Fe(12.7 ML)/Ag(001) multilayer. Within the error bar, the same magnetic profile was obtained as for the Au/Fe(13.5 ML)/Ag(1,1,6) sample. This confirms even stronger that the magnetic moment enhancement extends over 2–3 ML from the interface inside the Fe layer. However, the achieved resolution for obtaining the magnetic moment amplitude per slice is not sufficient to reveal any difference in the value of the magnetic moment that can be ascribed to the higher step density at the interface. Therefore, the results are considered identical for the Fe films grown on both Ag(1,1,6) and Ag(001) surfaces.

IV. DISCUSSION

Multiplying the derived msf values by $mm_0 = 2.1 \mu_B$ leads to the depth magnetic profile of the Fe $3d$ magnetic moment in μ_B per atom values. Figure 6 shows both magnetization depth profiles found for an Fe thickness of 13.5 and 5.9 ML. It can be clearly established from these results that at $T = 20$ K there is a magnetic moment enhancement in the first 2 to 3 ML from the interface. Note that the error bars in Fig. 6 are linked to a range allowing us to refine the data measured at different energies and for different configurations providing there is an enhancement of the magnetic moment at the interfaces with respect to the center of the film (see Fig. 4). We do not show the profile with monolayer resolution, i.e., obtained for $mm = 13$ or $mm = 6$, because the large number of parameters involved makes such model calculations unwieldy.

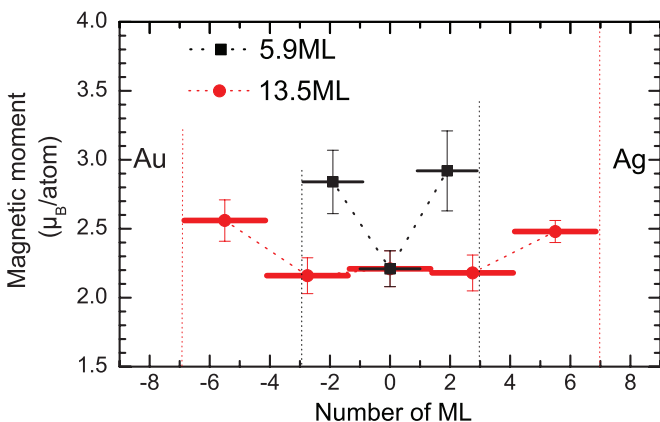


FIG. 6. (Color online) Depth magnetization profile obtained in both configurations for 5.9 and 13.5 ML of Fe deposited on Ag(1,1,6) and covered by 17 ML of Au. Length of the horizontal bars corresponds to the slice thickness, i.e., the number of atomic layers over which the magnetic moment is integrated. The vertical error bars correspond to different fit averages obtained for different energies and different configurations. Dashed lines represent interfaces with Ag (right) and Au (left).

It is well known that magnetization at the surface/interface depends on temperature stronger than for the bulk (or in the center of a thick film^{44,45}). Thus the values of the magnetic moment at the surface/interface and in the center of thick film become less different with increasing temperature. At a sufficiently high temperature the magnetic moment at the surface/interface can be even smaller than for the bulk. However, the temperature dependence of magnetization becomes more homogeneous across the film with decreasing film thickness because the reduced exchange interaction extends over several atomic layers. Since the effect of reduced symmetry at the surface/interface on the magnetic moment is more local, the magnetic moment increased at the interfaces with respect to the film center is expected to persist even for a few monolayers thick film. This is what we observe for our 13.5 and 5.9 ML thick samples if the XRMR experiment is performed at RT. Surprisingly, there is no big difference between the temperature dependence of the magnetic moment at the interfaces and in the center of the film 13.5 ML thick. However, with the accuracy of our method for the absolute values of magnetic moments (5%–11%), it is difficult to determine quantitatively the temperature dependence of the interfacial moment enhancement which can be small, especially for such low thicknesses, where the magnetization changes by 12%–20% within the temperature range from 4 to 300 K (see, for example, Ref. 9).

Also, we have shown that the accuracy is not good enough to evidence differences between the enhancement of the magnetic moment at a flat surface and at a stepped surface. This is why, in the following, the results are compared with a theoretical investigation that assume flat surfaces.

The enhancement of the magnetic moment of Fe at Ag and Au interfaces was theoretically predicted a long time ago. The increased moment is predicted to extend over the three first atomic layers of Fe with an average value of about $2.6 \mu_B$.^{46,47} Some experiments report agreement with this prediction,^{8,9} but only indirectly (i.e., by showing that the average magnetization over an entire magnetic layer of Fe is increased when the thickness is decreased). Determining the depth magnetic profile of a thin Fe layer with a spatial resolution of approximately 2–3 ML allows the direct detection of the magnetic moment enhancement near the interfaces. The enhanced magnetic moment for ~ 3 ML at the interface is found to be approximately $2.6 \pm 0.1 \mu_B$ per layer for the 13.5 ML thick film (see Fig. 6). Assuming the theoretically predicted magnetic moment value for the interfacial Fe atomic layer of 2.98 – $3.01 \mu_B$,^{1–3} an approximate result could be $2.4 \mu_B$ (i.e., a slightly increased moment) in the second and third atomic layers, which is also in good agreement with theoretical predictions.^{1–3} This averaged value compares well with the amount derived by SQUID for 2.9 ML films on a flat Ag surface ($2.67 \mu_B$).⁸ This is also in good agreement with the theoretical value ($2.78 \mu_B$) averaged over two Fe monolayers on Ag(001)⁴⁸ and with the value for one Fe monolayer sandwiched between two Ag films ($2.80 \mu_B$) and Au films ($2.92 \mu_B$).⁴⁸

Our results show that the enhancement of the magnetic moment at both interfaces (Au/Fe and Fe/Ag) is nearly the same. Although it is in a good agreement with theory, we cannot exclude that this can be due to a presence of Ag in the Au/Fe interface. It is known that Ag can flow to the top of an Fe

layer during the growth. Moreover, we cannot exclude that for the very interface atomic layer the magnetic moment is larger than the value we report for the interface slices. Especially since symmetry at the step edges is lower than that at the flat surfaces, it can cause the orbital magnetic moment to be larger at the vicinal surface. However, even a large increase of a small orbital contribution to the total magnetic moment cannot be resolved with the accuracy of our method. Finally, averaging the magnetization over the entire Fe thickness for both 13.5 and 5.9 ML, the total magnetic moments per Fe atom are 2.32 and 2.65 μ_B , respectively. These results are in a good agreement with the results found by Bland *et al.*⁹ for approximately 10 and 5.5 ML of Fe on Ag(001), respectively.

V. SUMMARY

In summary, a depth-resolved magnetic profile showing the enhancement of the magnetic moment at both Au and Ag interfaces at $T = 20$ K has been derived by soft XMRM applied to Au/Fe/Ag(1,1,6) and Au/Fe/Ag(001) samples.

This investigation confirms the high spatial resolution of the method necessary for describing the magnetic profile across a ferromagnetic thin film. Robust magnetization profiles have been determined using two different configurations displaying a strong difference in the angular dependence of the asymmetry. Despite a limited q space in the soft x-ray range (although measurements were performed up to $\theta = 0.85^\circ$), the spatial resolution is in the 2 ML range. It is difficult to detect an effect on the vicinal surface with respect to a flat surface on the magnetic moment at the immediate interface.

ACKNOWLEDGMENTS

Technical support from H. Menge and W. Greie at the Max-Planck-Institut für Mikrostrukturphysik, S. Garaudee at the Institut Néel, and R. Gaudemer at SOLEIL are acknowledged. We also thank E. Otero and P. Ohresser from DEIMOS beam line at SOLEIL for the XMCD measurements.

*jean-marc.tonnerre@grenoble.cnrs.fr

†mprzybyl@mpi-halle.de

- ¹S. Ohnishi, M. Weinert, and A. J. Freeman, *Phys. Rev. B* **30**, 36 (1984).
²R. Richter, J. G. Gay, and J. R. Smith, *Phys. Rev. Lett.* **54**, 2707 (1985).
³S. Blügel, B. Drittler, R. Zeller, and P. H. Dederichs, *Appl. Phys. A* **49**, 547 (1989).
⁴C. Li, A. J. Freeman, and C. L. Fu, *J. Magn. Magn. Mater.* **75**, 201 (1988).
⁵J. Tyson, A. H. Owens, J. C. Walker, and G. Bayreuther, *J. Appl. Phys.* **52**, 2487 (1981).
⁶J. Korecki and U. Gradmann, *Phys. Rev. Lett.* **55**, 2491 (1985); *Hyperfine Interact.* **28**, 931 (1986).
⁷M. Przybylski, U. Gradmann, and K. Krop, *Hyperfine Interact.* **57**, 2045 (1990).
⁸C. L. Wooten, J. Chen, G. A. Mulhollan, J. L. Erskine, and J. T. Markert, *Phys. Rev. B* **49**, 10023 (1994).
⁹J. A. C. Bland, C. Daboo, B. Heinrich, Z. Celinski, and R. D. Bateson, *Phys. Rev. B* **51**, 258 (1995).
¹⁰R. Stephan, A. Mehdaoui, F. Ott, and P. Wetzel, *J. Magn. Magn. Mater.* **320**, 3378 (2008).
¹¹J. Vogel, A. Fontaine, V. Cros, F. Petroff, J.-P. Kappler, G. Krill, A. Rogalev, and J. Goulon, *Phys. Rev. B* **55**, 3663 (1997).
¹²K. Amemiya, S. Kitagawa, D. Matsumura, H. Abe, T. Ohtaa, and T. Yokoyama, *Appl. Phys. Lett.* **84**, 936 (2004).
¹³M. Przybylski, *Hyperfine Interact.* **113**, 135 (1998).
¹⁴M. R. Fitzsimmons and C. F. Majkrzak, in *Modern Techniques for Characterizing Magnetic Materials*, edited by Y. Zhu (Springer, New York, 2005).
¹⁵J.-M. Tonnerre, E. Jal, E. Bontempi, N. Jaouen, M. Elzo, S. Grenier, H. L. Meyerheim, and M. Przybylski, *Eur. Phys. J. Special Topics* **208**, 177 (2012).
¹⁶D. Haskel, E. Kravtsov, Y. Choi, J. C. Lang, Z. Islam, G. Srajer, J. S. Jiang, S. D. Bader, and P. C. Canfield, *Eur. Phys. J. Special Topics* **208**, 141 (2012).

- ¹⁷L. Séve, N. Jaouen, J.-M. Tonnerre, D. Raoux, F. Bartolomé, M. Arend, W. Felsch, A. Rogalev, J. Goulon, C. Gautier, and J. F. Béar, *Phys. Rev. B* **60**, 9662 (1999).
¹⁸J. Geissler, E. Goering, M. Justen, F. Weigand, G. Schütz, J. Langer, D. Schmitz, H. Maletta, and R. Mattheis, *Phys. Rev. B* **65**, 020405(R) (2001).
¹⁹N. Jaouen, J. M. Tonnerre, D. Raoux, E. Bontempi, L. Ortega, M. Muenzenberg, W. Felsch, A. Rogalev, H. A. Durr, E. Dudzik, G. van der Laan, H. Maruyama, and M. Suzuki, *Phys. Rev. B* **66**, 134420 (2002).
²⁰T. Ohkochi, K. Mibu, and N. Hosoito, *J. Phys. Soc. Jpn.* **75**, 104707 (2006).
²¹S. D. Brown, L. Bouchenoire, P. Thompson, R. Springell, A. Mirone, W. G. Stirling, A. Beesley, M. F. Thomas, R. C. C. Ward, M. R. Wells, S. Langridge, S. W. Zochowski, and G. H. Lander, *Phys. Rev. B* **77**, 014427 (2008).
²²S. Roy, M. R. Fitzsimmons, S. Park, M. Dorn, O. Petravic, Igor V. Roshchin, Z.-P. Li, X. Batlle, R. Morales, A. Misra, X. Zhang, K. Chesnel, J. B. Kortright, S. K. Sinha, and I. K. Schuller, *Phys. Rev. Lett.* **95**, 047201 (2005).
²³S. Brück, G. Schütz, E. Goering, X. Ji, and K. M. Krishnan, *Phys. Rev. Lett.* **101**, 126402 (2008).
²⁴J.-S. Lee, C.-C. Kao, H. Jang, K.-T. Ko, J.-H. Park, K. Rhie, and J.-Y. Kim, *J. Phys.: Condens. Matter* **23**, 256001 (2011).
²⁵J. W. Freeland, J. Chakhalian, A. V. Boris, J.-M. Tonnerre, J. J. Kavich, P. Yordanov, S. Grenier, P. Zschack, E. Karapetrova, P. Popovich, H. N. Lee, and B. Keimer, *Phys. Rev. B* **81**, 094414 (2010).
²⁶H. L. Meyerheim, J.-M. Tonnerre, L. M. Sandratskii, H. C. N. Tolentino, M. Przybylski, Y. Gabi, F. Yildiz, X. L. Fu, E. Bontempi, S. Grenier, and J. Kirschner, *Phys. Rev. Lett.* **103**, 267202 (2009).
²⁷C. E. Viol Barbosa, H. L. Meyerheim, E. Jal, J.-M. Tonnerre, M. Przybylski, L. M. Sandratskii, F. Yildiz, U. Staub, and J. Kirschner, *Phys. Rev. B* **85**, 184414 (2012).

- ²⁸S. Brück, S. Treiber, S. Macke, P. Audehm, G. Christiani, S. Soltan, H.-U. Habermeier, E. Goering, and J. Albrecht, *New J. Phys.* **13**, 033023 (2011); K. Zafar, P. Audehm, G. Schütz, E. Goering, M. Pathak, K. B. Chetry, P. R. LeClair, and A. Gupta, *Phys. Rev. B* **84**, 134412 (2011).
- ²⁹D. Haskel, G. Srajer, J. C. Lang, J. Pollmann, C. S. Nelson, J. S. Jiang, and S. D. Bader, *Phys. Rev. Lett.* **87**, 207201 (2001).
- ³⁰N. Awaji, K. Noma, K. Nomura, S. Doi, T. Hirono, H. Kimura, and T. Nakamura, *J. Phys.: Conf. Series* **83**, 012034 (2007).
- ³¹J. Li, M. Przybylski, F. Yildiz, X. D. Ma, and Y. Z. Wu, *Phys. Rev. Lett.* **102**, 207206 (2009).
- ³²U. Bauer and M. Przybylski, *Phys. Rev. B* **81**, 134428 (2010).
- ³³M. Przybylski, M. Dąbrowski, U. Bauer, M. Cinal, and J. Kirschner, *J. Appl. Phys.* **111**, 07C102 (2012).
- ³⁴U. Bauer, M. Dąbrowski, M. Przybylski, and J. Kirschner, *J. Magn. Magn. Mater.* **323**, 1501 (2011).
- ³⁵N. Jaouen, J.-M. Tonnerre, G. Kapoujian, P. Taunier, J.-P. Roux, D. Raoux, and F. Sirotti, *J. Synch. Radiat.* **11**, 353 (2004).
- ³⁶M. Sacchi, N. Jaouen, H. Popescu, R. Gaudemer, J.-M. Tonnerre, S. G. Chiuzbaian, C. F. Hague, A. Delmotte, J.-M. Dubuisson, G. Cauchon, B. Lagarde, and F. Polack, *J. Phys.: Conf. Series* **425**, 072018 (2013).
- ³⁷M. Elzo, E. Jal, O. Bunau, S. Grenier, Y. Joly, A. Ramos, H. C. N. Tolentino, J.-M. Tonnerre, and N. Jaouen, *J. Magn. Magn. Mat.* **324**, 105 (2012).
- ³⁸J. J. Hoyt, D. de Fontaine, and W. K. Warburton, *J. Appl. Crystallogr.* **17**, 344 (1984).
- ³⁹J.-M. Tonnerre, L. Séve, D. Raoux, G. Soullié, B. Rodmacq, and P. Wolfers, *Phys. Rev. Lett.* **75**, 740 (1995).
- ⁴⁰C. T. Chen, Y. U. Idzerda, H.-J. Lin, N. V. Smith, G. Meigs, E. Chaban, G. H. Ho, E. Pellegrin, and F. Sette, *Phys. Rev. Lett.* **75**, 152 (1995).
- ⁴¹P. Ohresser, E. Otero, F. Choueikani, S. Stanescu, F. Deschamps, L. Ibis, T. Moreno, F. Polack, B. Lagarde, F. Marteau, F. Scheurer, L. Joly, J.-P. Kappler, B. Muller, and Ph. Sainctavit, *J. Phys.: Conf. Series* **425**, 212007 (2013).
- ⁴²J.-M. Tonnerre, *Lectures Notes Magnetism and Synchrotron Radiation*, edited by E. Beaurepaire, B. Carrière, and J.-P. Kappler (Les Editions de Physique, Mittelwihr, 1996).
- ⁴³D. R. Lee, S. K. Sinha, C. S. Nelson, J. C. Lang, C. T. Venkataraman, G. Srajer, and R. M. Osgood III, *Phys. Rev. B* **68**, 224410 (2003).
- ⁴⁴G. T. Rado, *Bull. Am. Phys. Soc.* **2**, 127 (1957).
- ⁴⁵J. Korecki, M. Przybylski, and U. Gradmann, *J. Magn. Magn. Mater.* **89**, 325 (1990).
- ⁴⁶J. Izquierdo, A. Vega, L. C. Balbás, D. Sánchez-Portal, J. Junquera, E. Artacho, J. M. Soler, and P. Ordejón, *Phys. Rev. B* **61**, 13639 (2000).
- ⁴⁷M. Benoit, C. Langlois, N. Combe, H. Tang, and M.-J. Casanove, *Phys. Rev. B* **86**, 075460 (2012).
- ⁴⁸C. L. Fu, A. J. Freeman, and T. Oguchi, *Phys. Rev. Lett.* **54**, 2700 (1985).